Mathematical model of blood glucose dynamics by emulating the pathophysiology of glucose metabolism in type 2 diabetes mellitus

Nelida Elizabeth López-Palau
Instituto Potosino de Investigacion Cientifica y Tecnologica
José Manuel Olais-Govea (olais@tec.mx)
Instituto Tecnologico y de Estudios Superiores de Monterrey https://orcid.org/0000-0002-1321-1822

Research

Keywords: type 2 diabetes pathophysiology, compartmental mathematical models, pharmacokinetic-pharmacodynamic modeling approach, parameter fitting

Posted Date: March 16th, 2020

DOI: https://doi.org/10.21203/rs.3.rs-17229/v1

RESEARCH

Mathematical model of blood glucose dynamics by emulating the pathophysiology of glucose metabolism in type 2 diabetes mellitus

Nelida E López-Palau[1,2*] and José Manuel Olais-Govea[2,3]

*Correspondence:
nelida.lopez@ipicyt.edu.mx
[1]División de Matemáticas Aplicadas, IPICyT, Camino a la Presa San José No. 2055, Lomas Cuarta Sección, 78216 San Luis Potosí, SLP., Mexico
Full list of author information is available at the end of the article

Abstract

Background.- This work addresses a physiological-based mathematical model of blood glucose dynamics in Type 2 *Diabetes Mellitus* (T2DM). **Results.-** The model emulates the pathophysiology of the T2DM metabolism including the gastric emptying effect and the enhancing effect on insulin due to the incretin hormones. Its mathematical structure considers a model of blood glucose dynamics of healthy humans developed with a physiological-based pharmacokinetic-pharmacodynamic approach. Then, the mathematical functions, representing the metabolic rates with a relevant contribution to hyperglycemia, are individually fitted to clinical data of T2DM patients. Methodologically, it allows emulating the pathophysiology of the T2DM condition. Numerically, the resulting model simulates successfully a programmed graduated intravenous glucose test and different-doses oral glucose tolerance tests. **Conclusion.-** The comparison between simulations and clinical data shows a good agreement description of the blood glucose dynamics in T2DM and, it opens the likelihood of using this model to develop model-based controllers for blood glucose regulation in T2DM.

Keywords: type 2 diabetes pathophysiology; compartmental mathematical models; pharmacokinetic-pharmacodynamic modeling approach; parameter fitting

Background

For some decades, mathematical models have been used in biological sciences to understand diverse aspects of *diabetes mellitus* (DM) [1]. For example, DM progression [2, 3], diagnostic test evaluations [4, 5], long-term micro and macrovascular complications [6, 7],

and blood glucose dynamics [8, 9, 10], among others, have been modeled. Particularly, mathematical models to emulate blood glucose dynamics in DM have been classified, according to the complexity of their description, in two major groups [11]. The first group considers the whole-body models developed under a pharmacokinetic-pharmacodynamic (PKPD) approach which is characterized by being structurally simple with a limited physiological interpretation. The second group considers the physiological-based PKPD (PB-PKPD) models, which mathematically describe the physiological interactions between different subsystems of the human body. Due to its structural simplicity, most of the models in the literature are PKPD [1]. Although these models are widely used they do not include most of the processes responsible for glucose homeostasis. Hence, its use to model complex processes in DM, such as the DM pathophysiology is limited and, it induces a trend toward the development of PB-PKPD models [1]. These models have focused on emulating the metabolic processes involved in glucose homeostasis and are usually organ-based. Moreover, the PB-PKPD models of blood glucose dynamics in type 1 DM (T1DM) have been useful to synthesize model-based controllers for blood glucose regulation in T1DM [12, 13, 14, 15, 16]. However, type 2 DM (T2DM) affects multiple subsystems of the body and, consequently, the mathematical representation of the metabolic abnormalities in T2DM is challenging [17].

One of the most widely used PB-PKPD models was performed by Sorensen [10]. This organ-based compartmental model emulates the blood glucose dynamics of a healthy human by considering the main glucose metabolic rates as mathematical functions. In this model, each mathematical function was individually fitted to a set of clinical data of healthy people where the metabolic response of the patients was measured for different stimuli. Then, the physiology of the main metabolic rates of a healthy human body was mathematically reproduced. Although the Sorensen's model is quite robust, it has some limitations. For instance, the model does not include the blood glucose and insulin dynamics in the pancreas, instead, a single function representing the pancreatic insulin release rate is connected to the bloodstream. The above does not represent the physiology of the human body. In addition, the model does not consider the effect of gastric emptying, therefore, the blood glucose dynamics after oral glucose intake and the potentiating-insulin effect of the incretin hormones cannot be reproduced.

An extension of the Sorensen's model, which covers its main limitations, was proposed by Alverhag and Martin [9]. Thus, the model included two ordinary differential equations

(ODE) to quantify, by means of mass balance, the time-variation of the blood glucose and insulin in the pancreas. Additionally, the gastric emptying process and the enhancing effect on insulin due to the incretin hormones were included by considering two new subsystem attached to the model. Furthermore, Alverhag and Martin hypothesize that a model of the blood glucose dynamics in T2DM can be developed by identifying the parameters of the mathematical functions representing the metabolic rates related to the pathophysiology of this condition [9]. Then, in 2011 Vahidi *et al.* used a nonlinear optimization approach to identify some parameters of the Sorensen's model from a single data set of an oral glucose tolerance test (OGTT) in T2DM patients [8]. The methodology used by the authors to estimated the model parameters was a non-global optimization method. Then, even though the system in Vahidi *et al.* acceptably reproduces the OGTT, the set of identified parameters that minimize the error between clinical data and the system may not be unique. Therefore, it cannot be assured that, individually, the metabolic functions containing the identified parameters numerically can emulate the pathophysiology the T2DM.

Consequently, this article propose a PB-PKPD model of the blood glucose dynamics in T2DM, where some mathematical functions representing metabolic rates of the body, are individually fit to emulate the pathophysiology of the T2DM. Moreover, the effect of the gastric emptying and the enhancing effect of insulin due to the incretin hormones are included to reproduce the blood glucose dynamics after oral glucose intake. To achieve this, the mathematical model of the blood glucose dynamics in a healthy human body, proposed in Alvehag and Martin [9], will be described as a set of 28-dimensional ODE. From the ODE set, the mathematical functions representing the impaired metabolic rates in T2DM were individually fitted to clinical data of T2DM patients by using the least-squares method (LSM). The clinical data were taken from several clinical tests where direct measurements of the tissues or organs response to local changes in solutes concentration were made. The resulting model was numerically simulated to test its ability to reproduce the blood glucose dynamic in T2DM patients for different inputs and initial conditions. Finally, the error between the simulation and the clinical data of the T2DM patients is quantified by using a statistical function.

Methodology

The mathematical model in Alverhag y Martin, is a nonlinear dynamic system consisting of four clustered subsystems [9]. The subsystems are compartmental representations of the

human body, where each compartment represents an organ or tissue where an important process of mass exchange is carried out. The compartments are interconnected through the blood flow. Then, by means of a mass balance in the compartments, each of the subsystems quantifies the concentration of one solute (*i.e.* glucose, insulin, glucagon, or incretins). A detailed explanation of the system and its nomenclature can be found in the Appendix.

The system is a set of 28 ODE composed of nonlinear continuous functions. Therefore, it follows that the solution of the system ($x(t)$) exists in a domain $\mathbb{D}$ as long as the initial conditions are in $\mathbb{D}$. As a methodological approach in this work, the solution of the system is represented from a state-space theory as the vector:

$$\begin{aligned} x = [&G_{BV},\, G_{BI},\, G_H,\, G_L,\, G_K, G_{PV},\, G_{PI},\, G_G,\, G_{PN}, \\ &I_B,\, I_H,\, I_L,\, I_K,\, I_{PV},\, I_{PI},\, I_G,\, I_{PN},\, \Gamma^N,\, \omega,\, \omega_G, \\ &M^I_{HGP},\, M^I_{HGU},\, F_2,\, P,\, I,\, Q,\, G_s,\, r_{OGA}] \end{aligned} \tag{1}$$

where $x(t) = (x_1(t), x_2(t), ..., x_{28}(t)) \in \mathbb{D} \subset \mathbb{R}^{28}$ is semi-defined positive, which means that it belongs to the set $\mathbb{R}^{28}_+$. Using the state definition in the equation (1), the system is defined as:

$$\dot{x}(t) = F(x(t); \pi, \eta), \;\; x(t_0) = x_0 \in \mathbb{D} \tag{2}$$

where the vector field $F(x(t); \pi, \eta) :\rightarrow \mathbb{R}^{28}$ determines the time evolution of $x(t)$ starting at initial condition (x_0) in the initial time (t_0), and $\pi \in \Pi \subset \mathbb{R}^{46}$ contains the parameters in the functions representing hemodynamical processes, while $\eta \in$H$\subset \mathbb{R}^{67}$ contains the parameters in the functions representing the metabolic rates of the system. The parameter values of the system in the equation (2) can be found in the Appendix.

Model simulation and initialization

The mathematical model in the equation (2) successfully simulate the blood glucose dynamics of a healthy human body after intravenous glucose infusion and oral glucose intake [9]. For the above, an input to the system is considered containing: *i)* a continuous intravenous glucose infusion rate (r_{IVG}), which is introduced to the system as an insulin rate in mg/dL/min, and *ii)* an oral glucose intake (OGC_0), which is introduced to the system in mg and it is connected to the gastric emptying process (see Appendix). The output of the system (y) is considered as $x_6 = G_{PV}$ and $x_{14} = I_{PV}$, whose meaning concerns to glucose

and insulin vascular concentration in peripheral tissues, respectively. The time evolution of y is used to compare the model simulation with clinical data where the glucose and insulin concentrations are taken from a blood sample of the patient's forearm during a test. For all the simulations, the model in the equation (2) was numerically solved by using variable step in the function *ode45 (Dormand-Prince)* of Matlab. The simulation time was defined as the time length of the clinical trial.

For model initialization, the basal condition (x^B) and x_0 were computed from the solute concentrations in the fasting state of the patients. The condition x^B is determine as the average fasting glucose and insulin concentration from the blood samples collected over several days, this is x_6^B and x_{14}^B respectively. The condition x_0 is determined as the fasting glucose and insulin concentrations from a blood sample at time zero of the clinical test; this is $x_6(0)$ and $x_{14}(0)$, respectively. Mathematically, the fasting state has a physiological correspondence with the steady state of the system (x^*) in the equation (2), this is:

$$F(x^*;\pi;\eta) = 0 \tag{3}$$

then, since interstitial, arterial, and venous concentrations are the same at the steady state, the peripheral vascular data for x^B and x_0 are computed from the arterial or venous data. The remaining 26 components of x^B and x_0 are obtained from the solution of the equation (3).

Metabolic rates of the model

The model subsystems are coupled by the functions representing the metabolic rates of the glucose, insulin, glucagon, and incretins. These metabolic rates are mathematically modeled as constant functions, linear functions of the mass accumulation in the compartments, or multiplicative functions of the metabolic basal rate. Specifically, the metabolic rates in the glucose and glucagon subsystems are multiplicative functions with the following general form:

$$r = M^G M^I M^\Gamma r^B \tag{4}$$

where r^B represents the basal value of the metabolic rate r, and each M is the isolated effect of the normalized concentration of glucose (M^G), insulin (M^I) and glucagon (M^Γ) of the normalized metabolic rate ($r^N = r/r^B$). The above implies that $M^G = M^I = M^\Gamma = 1$ when the glucose, insulin and glucagon are basal, therefore $r = r^B$. To represent the characteristic

sigmoidal non-linearities of biological data correlations, excepting the isolated effects that are states of the system in the equation (2) (*i.e.* M^I_{HGP} and M^I_{HGU}), all the isolated effects are hyperbolic tangent functions of some normalized component of the state, this is:

$$M(x_i^N) = \eta_{j_1} + \eta_{j_2} \tanh(\eta_{j_3}(x_i^N + \eta_{j_4})) \tag{5}$$

where $x_i^N = x_i/x_i^B$ for $i \in \{1,2,...28\}$ and $\eta_{j_1}, \eta_{j_2}, ..., \eta_{j_4} \in H$ with $j_1, j_2 ... j_4 \in \mathbb{N} \leq 67$ are dimensionless parameters. A list containing the nominal values of the η parameters can be found in the additional files. By using these values, the system in the equation (2) simulate the blood glucose dynamics after an intravenous glucose infusion or an oral glucose intake in a healthy human body [9]. For the mathematical modelling of the blood glucose dynamics of T2DM, the pathophysiology of T2DM must be emulated by modifying the value of the parameters of the functions representing the metabolic rates responsible of the characteristic hyperglycemia. The above will be described in the *Curve Fitting* section.

Curve fitting

For decades, different studies have identified the metabolic problems associated with the progression of T2DM in healthy humans [18, 19]. It has been found that these problems are associated with the metabolism of fats and carbohydrates [18, 19], being the metabolism of the latter, the object of study of this work.

Mainly, the pathophysiology of the T2DM is characterized by [18]: *i)* insulin resistance, defined as an impaired effect of insulin on glucose uptake by peripheral tissues, *ii)* excessive hepatic glucose production, and *iii)* β-cell dysfunction, represented by an impaired pancreatic insulin release. Then, the mathematical functions of the system in the equation (2) modelling the aforementioned metabolic rates are: the effect of insulin in peripheral glucose uptake (*i.e.* M^I_{PGU}), the effect of glucose, insulin and glucagon on the hepatic glucose production (*i.e.* M^G_{HGP}, $M^{I_\infty}_{HGP}$ and $M^{\Gamma_0}_{HGP}$, respectively), and the pancreatic insulin release (*i.e.* r_{PIR}). Since a small variation in the parameters of these metabolic rates results in a variation of the solute concentrations in the model, in the following sections, the terminology of the sensitivity analysis from Khalil will be adopted [20]. Therefore, the above metabolic rates will be called *sensitive metabolic rates*.

In what it follows, all sensitive metabolic rates were fitted to available clinical data of T2DM patients, while the parameters of the rest of the metabolic rates remained at the values defined in the Appendix. Explicitly, the fitting of r_{PIR} is supported by several clinical

tests where a decrease of the first phase of pancreatic insulin release in patients with T2DM is exhibited [21, 22, 23]. The above is consistent with the early proposal to induce a partial impairment on insulin release from the labil compartment, in order to decrease the first phase of insulin release in T2DM patients [24]. Due to the above, the functions representing the first phase of insulin release (X and P_∞), and the time-variation of the amount of labil insulin ready to be released, were studied by means a sensitivity analysis as in Khalil (2002) [20]. From this analysis, the parameters that shows a major contribution to the sensitivity on solution $x(t;\eta,\pi_0)$ were selected to fit r_{PIR}.

Static and dynamic fitting approach

To solve the parameter fitting problem, two things are required:

1 A set of clinical data in T2DM patients.

2 A mathematical method to fit such data to the function representing the sensitive metabolic rates.

The set of clinical data to fit the isolated effects functions was obtained from selected clinical tests of T2DM patients, where direct measurements of tissues or organs response to local changes in solutes concentration were made. The selection criteria of the tests was as follows: the conditions of the test must be consistent with those originally considered for mathematical modeling in Sorensen [10] and the patients must have not other significant medical history than T2DM. The conditions of the clinical tests are compiled in Table 1. Particularly, to fit r_{PIR} the clinical data from a graded glucose step-response with the isolated perfused pancreas in T2DM patients can not be collected. Then, the selected parameters of this metabolic rate were identified using clinical data from an input-output approach of the system in the equation (2). The data was taken from an OGTT in DeFronzo *et al.* [25], where the plasma glucose and insulin response to oral intake were measured in nine T2DM subjects after the consumption of 1g/kg body-weight of oral glucose.

The mathematical method used to fit the functions to clinical data is LSM. In general, the LSM lies that the following relation is fulfilled [26]:

$$\bar{y} = g(z,U) \tag{6}$$

where z and $\bar{y}$ are vectors containing n observations, and $U \in \mathbb{R}^{p\times 1}$ is a vector of p unknown parameters of the sensitive metabolic rate. To estimate U the n values of g are computed for all z. Then, $\hat{U}$ is the estimation of the vector of parameters corresponding to U that

minimizes the residual sum of squares of an objective function $Q(U)$ over some feasible the vector of parameters $U \geq 0 \subset \Theta$. The isolated effects of the sensitive metabolic rates were fitted to clinical data by a static approach of the LSM. After that, a dynamical approach of the LMS was used to identify the parameters of the r_{PIR} function. In what follows, both approaches will be described.

In the static approach, the unknown parameters from the equation (5) are grouped as $U = [\eta_{j_1}, \eta_{j_2}, \eta_{j_3}, \eta_{j_4}]^T$. The vector $\hat{U}$ is estimated with an iterative process using the following objective function:

$$Q(U) = \sum_{k=1}^{n} (y_k - M(z_k, U))^2 \tag{7}$$

where y_k is clinical data of the average of the normalized metabolic rate in T2DM patients respect its basal value in [9], and z_k is clinical data of the average of the normalized solute concentration taken from the forearm. The minimization of the objective function in the equation (7) was numerically solved with the function *lsqcurvefit* of the optimization toolbox of MatLab. The iterative algorithm used to find $\hat{U}$ was 'trust-region reflective' proposed in Li (1993) [45]. After fitting, (z_k,y_k) are graphically compared with the fitted isolated effects functions. Then, the values in $\hat{U}$ replaced its respective nominal values defined in the Appendix.

In the dynamical approach the selected parameters from r_{PIR} were grouped as $U = [\eta_{l_1}, \eta_{l_2}, \eta_{l_3}, \eta_{l_4}, \eta_{l_5}, \eta_{l_6}]^T$ with $l_1, l_2, ...l_6 \in \mathbb{N} \leq 67$. The vector $\hat{U}$ was estimated with an iterative process using the following objective function:

$$Q(U) = \sum_{k=1}^{n} \left(\left(\frac{y_{1k} - f_1(z_k, U)}{w_1} \right)^2 + \left(\frac{y_{2k} - f_2(z_k, U)}{w_2} \right)^2 \right)^{1/2} \tag{8}$$

where y_{1k} and y_{2k} are clinical data obtained from the average of glucose and insulin concentrations,respectively, taken at the z_k time, the weights w_1 and w_2 are the average of the basal glucose and insulin concentrations, respectively, and $f_1 = x_6(z_k, U)$, $f_2 = x_{14}(z_k, U)$ were obtained from the model simulation. The above clinical data was taken from DeFronzo *et al.* [25]. The LSM problem in the equation (8) was numerically solved using the function *fmincon* of the optimization toolbox of MatLab with the iterative algorithm 'interior-point'. After the identification of the parameters of r_{PIR}, the values in $\hat{U}$ from the static and dynamical approach replaced the nominal values of the parameters in the Appendix to emulate

the pathophysiology of T2DM. Therefore, hereinafter, the resulting model is called *T2DM model*.

Comparison of the T2DM model with clinical data

The T2DM model was numerically simulated for comparison with clinical test in T2DM where the blood glucose dynamics is observed after different stimuli. Considering that the route of glucose entry into the body plays an essential role overall glucose homeostasis [25], the T2DM model was simulated for the following test: *i*) a programmed graduated intravenous glucose infusion (PGIGI) test to account for rapid response of the intravenous infusions and *ii*) an OGTT considering a dose of 50 g of glucose (50g-OGTT) and a dose of 75 g of glucose (75g-OGTT) to account for blood glucose changes due to the gastric emptying process and the incretins effects.

In the PGIGI the glucose was administrated through r_{IVG}, while $r_{OGA} = 0$. The duration of the test was 270 min distributed as follows: a basal sampling period was considered were $r_{IVG} = 0$ from 0-30 min, after this, the steps of intravenous glucose infusion were introduced as $r_{IVG} = 1,2,3,4,6$ and 8 mg/dL/min for a period of 40 min each one. The clinical data were taken from Carpentier *et al.* [27], and the conditions for model simulation were $G^B_{PV} = G_{PV}(0) = 157.5$ mg/dL and $I^B_{PV} = I_{PV}(0) = 13.02$ mU/L.

For the OGTT test, the duration of the simulation was 180 min. The amount of glucose was introduced at minute zero trough OGC_0 and the input r_{IVG} was considering null. The clinical data for the 50g-OGTT were taken from Firth *et al.* [28], and the conditions for model simulation were OGC_0 =50 000 mg, $G^B_{PV} = G_{PV}(0) = 185$ mg/dL and $I^B_{PV} = I_{PV}(0) = 14$ mU/L. Additionally, the clinical data for the 75g-OGTT were taken from Mari *et al.* [29], and the conditions for model simulation were $OGC_0 = 75\,000$ mg, $G^B_{PV} = G_{PV}(0) = 176$ mg/dL and $I^B_{PV} = I_{PV}(0) = 11.2$ mU/L.

The difference between the clinical data and the model simulation was quantified with the following statistical expression:

$$\sigma = \sqrt{\frac{1}{n-1} S_e} \tag{9}$$

where $S_e = \sum_{s=1}^{n} (x_6(t_s) - G(t_s))^2$, and G is the glucose concentration taken from the T2DM patients at the time t_s. All the clinical test where different from those used for curve fitting.

Results and discussion

The clinical data that fulfills the conditions provided in Table 1 were taken from the references grouped in Table 2. The parameter set $\hat{U}$ for each isolated effect of the sensitive metabolic rate can be seen in Table 3. Furthermore, in Figure 1 it can be found a graphic representation of the curves that fit the isolated effects functions of the sensitive metabolic rates to the clinical data of Table 1. As can be seen, the curves in in Figure 1 do not necessarily pass through the point $(x_i^N, M(x_i)^N) = (1,1)$. This is because the isolated effects of the metabolic rates were normalized with respect to the basal value of the metabolic rates in [9], which correspond to a mathematical model of the blood glucose dynamics in a healthy human body. The above is justified by the fact that not all isolated effects of glucose, insulin, or glucagon on a metabolic rate are observed altered in T2DM patients. Since the metabolic rates are expressed as multiplier factors of the basal metabolic rate, the isolated effects that have not been observed altered in patients with T2DM will continue to be multiplier factors of the basal metabolic rate (r^B) of a healthy human body.

As can be seen in in Figure 1(a) the curve corresponding to M_{PGU}^I goes close to the point $(x_{15}^N, M_{PGU}^I(x_{15}^N)) = (1,1)$. The above means that the insulin-stimulated peripheral glucose uptake in a T2DM patient does not differ much from the one in a healthy human when the fasting hyperglycemia and basal insulin concentration are maintained in the T2DM patient. This characteristic of the T2DM has been previously reported in several articles [30, 31, 32, 33]. In contrast, as can be seen in in Figure 1(b), for $x_4^N = 1$, the value of M_{HGP}^G is greater than one, this means that considering basal hyperglycemia the hepatic glucose production is higher in T2DM patients compared to that observed in healthy humans. The above has been previously reported by various articles where the effect of glucose on the hepatic glucose production rate was verified for healthy control subjects and T2DM patients [34, 35]. Moreover, the hepatic insulin resistance, characteristic of the T2DM, is evident in Figures 1(b) and 1(c). This can be observed in the behavior of the curves for high values of the solute concentration, where, the hepatic glucose production can not be completely suppressed despite significant increment of the normalized glucose and insulin concentration in the liver. The above is consistent with clinical evidence where the blood glucose has an impaired ability to inhibit the hepatic glucose production at basal insulin and glucagon concentrations in T2DM [34, 35, 18], and the insulin concentration is ineffective to suppress the hepatic glucose production at basal glucose and glucagon concentrations in T2DM [39, 40, 25, 42]. Finally, the role of glucagon in hepatic glucose production in

T2DM patients can be seen in Figure 1(d). In this graphical representation, the behaviour of the function $M_{HGP}^{\Gamma_0}$ is consistent with the clinical data of patients with T2DM [44, 41]. The, it follows that by fitting the isolated effect functions to the clinical data, it is possible to individually emulate the pathophysiology of the T2DM.

After isolated effects fitting, a parameter set containing the parameters of r_{PIR} that show a greater contribution to the sensitivity on the solution $x(t;\eta,\pi_0)$ was selected. From the sensitive analysis the parameter selected parameter set was $\hat{U} = [\eta_{36}, \eta_{39}, \eta_{40}, \eta_{42}, \eta_{44}, \eta_{45}]^T$. The values of $\hat{U}$ that minimize the objective function in equation (8) can be seen in the Table 4. After replacing the nominal values of the parameters in the additional files for those in $\hat{U}$ in Tables 3 and 4 the system simulate the response to a 70g-OGTT. The results of the simulation and its comparison with clinical data from DeFronzo *et al.* [25] can be seen in Figure 2. As can be seen there is an acceptable approximation of the simulation curve to the clinical data. Moreover, almost all test the simulation remains within the bars of the standard error. It should be noted that even when y_{1k} and y_{2k} have different orders of magnitude, the emulation of both blood glucose and insulin was successfully achieved. This is mainly due to the addition of weight functions of weights in the objective function of the equation (8). As noted in the *Methodology* section, since there is no clinical data of the individual response of r_{PIR} measured against different stimuli, the dynamic approach used to fit r_{PIR} is based on an nonlinear optimization. As a result, the set of values obtained minimizes the objective function of the equation (8), nevertheless, it cannot be assured that the pathophysiology of the pancreatic insulin secretion in T2DM is individually emulated. However, due to the individual fitting of the isolated effects, the number of parameters to be identified by a dynamic approach is minimal. A proposal to avoid the above is to replace the pancreatic insulin subsystem with a model of the pancreas whose pathophysiology could be described by a set of clinical data of patients with T2DM.

After the metabolic rates fitting the resulting model (*i.e.* T2DM model) was simulated and compared with clinical data. In figure 3 can be seen the T2DM model response for the PGIGI test and the clinical data from Carpentier *et al.* [27]. As can be seen, the simulation of the T2DM model is not significantly different from the reported clinical data. Moreover, the absolute of the maximum difference between simulation and clinical data is 9.4 mg/dL. This is consistent with the obtained statistical value $\sigma = 5.37$ mg/dL for this test. It follows that the T2DM model can reproduce the step response of the blood glucose due to an intravenous glucose infusion input. Meanwhile, in the Figure 4 it can be seen the T2DM

model response of the OGTT for different doses. Similarly to the observed clinical data, the model response x_6 rises to a maximum peak approximately at 80 minutes after the stimulus of 50 g and 75 g. The statistical value σ for the 50 and 75g-OGTT is 16.84 mg/dL, and 13 mg/dL, respectively. As can be seen, after oral glucose intake, the response of the model for the OGTT test is relatively slow, showing a maximum peak at approximately 80 minutes after glucose stimulation. Compared with the results of the PGIGI, the increase in glycemia in the OGTT is slower. This is because the digestion process, after an oral glucose intake, induces a delay proportional to the glucose appearance rate in the gut. Furthermore, as can be seen in the figures 2 to 4 the basal blood glucose is slightly elevated compared to the concentration of a healthy subject. According to the World Health Organization guidance for diagnostic tests of DM, a fasting glucose concentration $\geq$126 mg/dL is characteristic of DM [46]. Moreover, the patients with this impaired blood glucose should undergo by a formal 75g-OGTT for DM diagnosis [46]. A representation of this test can be seen in the figure 4 where after two-hour postload glucose the dotted curve shown a glucose concentration $\geq$140 mg/dL. This is a characteristic behavior of T2DM that contrasts with that of a healthy subject, where the normal homeostatic glucose process results in a concentration of less than 140 mg/dL after two hours of the glucose intake.

Based on the values of the σ function, it can be establish that the model emulates with acceptable precision what is reported in the clinical data for PGIGI and OGTT. However, this model considers only the carbohydrate metabolism but not the fat metabolism. Therefore, the effect of free fatty acids on blood glucose dynamics is not included. Besides, the model does not consider the counter-regulatory effect of growth hormones, adrenaline, or cortisol. Nevertheless, the above can be considered later in the model by adding other subsystems for the free fatty acids dynamics and other metabolic functions to consider the effect of the missing hormones.

Conclusion

The main contribution of this article was derivating a model for T2DM including physiological features to emulate blood glucose dynamics. The modeling departs from a PB-PKPD modeling approach and the individual fitting of the sensitive metabolic rates allows us to capture the pathophysiology of the metabolic rates in T2DM. This gives way to successfully emulate the blood glucose dynamics of T2DM after a continuous intravenous

glucose infusion an oral glucose intake. As convincing numerical evidence of the above, Figures 3 and 4 show to what extent the T2DM model predicts the clinical data.

The individual fitting of the sensitive metabolic rates to clinical data ensures that the pathophysiology of T2DM is preserved, such that diverse scenarios might be predicted. For instance, this model can be used to determine an appropriate oral therapy for blood glucose regulation by connecting a PKPD model of a hypoglycemic drug (e.g. sulfonylureas, biguanides, thiazolidinediones, among others). Such is the case of the metformin therapy, where the targets metabolic rates were modified by adding a multiplicative factor in r_{HGP}, r_{PGU}, and r_{GGU} [47]. Furthermore, this model can be used to develop feedback model-based controllers for blood glucose regulation in T2DM patients. This idea triggers of the possibility to achieve the normoglycemia by means of single or combined therapy of oral hypoglycemic agents with an exogenous insulin input connected to r_{IVI}. Finally, a stark consequence of the physiological-based model structure is to consider structured or unstructured uncertainties, therefore, robust control techniques can be used, for instance, H_∞ theory.

Abbreviations

- **DM:** Diabetes Mellitus.
- **PKPD:** Pharmacokinetic-pharmacodynamic model.
- **PB-PKPD:** Physiological-based PKPD.
- **T1DM:** Type 1 Diabetes Mellitus.
- **T2DM:** Type 2 Diabetes Mellitus.
- **ODE:** Ordinary differential equations.
- **OGTT:** Oral glucose tolerance test.
- **LSM:** Least-squares method.
- **PGIGI** Programmed graduated intravenous glucose infusion.

Declarations

Ethics approval and consent to participate

Not applicable.

Consent for publication

Not applicable.

Availability of data and material

All data generated or analysed during this study are included in this published article.

Funding

This work was supported by the Sofía Kovalévskaia Foundation and the National Council of Science and Technology in México [grant number 262267].

Competing interests

The authors declare that they have no competing interests.

Author's contributions

NELP obtained, analyzed and interpreted the data, contributed with the comparison between the clinical data and the interpretation of them, wrote the supplemental material and the paper. JMOG wrote part of the paper and, supervised the results of the paper. All the authors contributed to the description of the theoretical framework and a discussion of the results.

Acknowledgements

Not applicable.

Author details

[1]División de Matemáticas Aplicadas, IPICyT, Camino a la Presa San José No. 2055, Lomas Cuarta Sección, 78216 San Luis Potosí, SLP., Mexico. [2]Tecnologico de Monterrey, Escuela de Ingeniería y Ciencias, Av. Eugenio Garza Sada 300, Lomas del Tecnológico, 78211 San Luis Potosí, SLP, Mexico. [3]Tecnologico de Monterrey, Writing Lab, TecLab, Vicerrectoriía de Investigación y Transferencia de Tecnología, Av. Eugenio Garza Sada 2501 Sur, Col. Tecnológico, 64849 N. L., Mexico.

References

1. Ajmera I, Swat M, Laibe C, Nové re NL, Chelliah V 2013 The impact of mathematical modeling on the understanding of diabetes and related complications. *CPT Pharmacometrics Syst Pharmacol*, **2**, e54.
2. Hardy T, Abu-Raddad E, Porksen N, De Gaetano A 2012 Evaluation of a mathematical model of diabetes progression against observations in the Diabetes Prevention Program. *Am J Physiol Endocrinol Metab*, **303**, E200.
3. de Winter W, DeJongh J, Post T, Ploeger B, Urquhart R, Moules I, Eckland D, Danhof M 2006 A mechanism-based disease progression model for comparison of long-term effects of pioglitazone, metformin and gliclazide on disease processes underlying Type 2 Diabetes Mellitus. *J. of Pharmacokinetics and Pharmacodynamics*, **33**, 313.
4. Mari A, Pacini G, Murphy E, Ludvik B, Nolan JJ 2001 A model-based method for assessing insulin sensitivity from the oral glucose tolerance test. *Diabetes Care*, **24**, 539.
5. Hovorka R, Chassin L, Luzio SD, Playle R, Owens DR 1998 Pancreatic beta-cell responsiveness during meal tolerance test: model assessment in normal subjects and subjects with newly diagnosed noninsulin-dependent diabetes mellitus. *The Journal of Clinical Endocrinology and Metabolism*, **83**, 744.
6. Boutayeb A & Twizell EH 2004 An age structured model for complications of diabetes mellitus in Morocco. *Simulation Modelling Practice and Theory* **12**, 77.

7. Bagust A, Beale S 2003 Deteriorating beta-cell function in type 2 diabetes: a long-term model. *QJM: An International Journal of Medicine*, **96**, 281.
8. Vahidi O, Kwok KE, Gopaluni RB, Sun L 2011 Developing a physiological model for type II diabetes mellitus. *Biochemical Engineering Journal*, **55**, 7.
9. K. Alvehag and C. Martin 2006 The feedback control of glucose: on the road to Type II diabetes, *Proceedings of the 45 IEEE Conference on Decision and Control*, San Diego, pp. 685-690
10. Sorensen JT 1985 A Physiological Model of Glucose Metabolism in Man and its use to Design and Assess Improved Insulin Therapies for Diabetes. *Ph.D. Thesis, Massachusetts Institute of Technology*.
11. Cedersund G & Strålfors P 2009 Putting the pieces together in diabetes research: towards a hierarchical model of whole-body glucose homeostasis. *European Journal of Pharmaceutical Sciences* **36**, 91-104.
12. Ekram F, Sun L, Vahidi O, Kwok E, Gopaluni RB 2012 A feedback glucose control strategy for type II diabetes mellitus based on fuzzy logic. *Can. J. Chem. Eng*, **90**, 1411-17.
13. Huang M, Li J, Song X, Guo H 2012 Modeling Impulsive Injec tions of Insulin: Towards Artificial Pancreas. *SIAM J. Appl. Math.*, **72(5)**, 1524.
14. Quiroz G, Flores-Gutiérrez CP, Femat R 2011 Suboptimal H_∞ hyperglycemia control on T1DM accounting biosignals of exercise and nocturnal hypoglycemia. *Optim. Control Appl. Meth.*, **32**, 239-252.
15. Femat R, Ruiz-Velazquez E, Quiroz G 2009 Weighting restriction for intravenous insulin delivery on T1DM patient via H_∞ control. *IEEE Trans. Autom. Sci. Eng.*, **6**, 239-247.
16. Parker RS, Doyle FJ, Ward JH and Peppas, N.A. 2000 Robust H_∞ glucose control in diabetes using a physiological model. *AIChE J*, **46**, 2537-2549.
17. Yamanaka Y, Uchida K, Akashi M, *et. al.* 2019 Mathematical modeling of septic shock based on clinical data. *Theor Biol Med Model* **16**, 5.
18. DeFronzo RA 2004 Pathogenesis of type 2 diabetes mellitus. *Medical Clinics*, **88**, 787-835.
19. Leahy JL. 2005 Pathogenesis of type 2 diabetes mellitus. *Archives of medical research*, **36**, 197-209.
20. Khalil HK 2002 Nonlinear Systems, third ed. *Prentice Hall*. New Jersey.
21. Kjems LL, Vølund A Madsbad S 2001 Quantication of betacell function during IVGTT in Type II and non-diabetic subjects: assessment of insulin secretion by mathematical methods. *Diabetología* **44**, 1339-1348.
22. Del Prato S 2003 Loss of early insulin secretion leads to postprandial hyperglycaemia. *Diabetologia*, **46**, M2-M8.
23. Ward WK, Bolgiano DC, McKnight B, Halter JB, Porte DJr 1984 Diminished B cell secretory capacity in patients with noninsulin-dependent diabetes mellitus. *J. Clin. Invest.*, **74(4)**, 1318-1328.
24. Grodsky GM, Curry D, Herbert L, Leslie B 1969 Further studies on the dynamic aspects of insulin release in vitro with evidence for a two-compartmental storage system. *Acta Diabetologica Latina*, **6**, 554-578.
25. DeFronzo RA, Gunnarsson R, Björkman O, Olsson M, Wahren J 1985 Effects of insulin on peripheral and splanchnic glucose metabolism in noninsulin-dependent (type II) diabetes mellitus. *J Clin Invest*, **76**, 149-155.
26. Jennrich RI, Ralston ML 1979 Fitting nonlinear models to data. *Annual Review of Biophysics and Bioengineering*, **8**, 195-238.
27. Carpentier A, Mittelman SD, Bergman RN, Giacca A, Lewis GF 2000 Prolonged elevation of plasma free fatty acids impairs pancreatic beta-cell function in obese nondiabetic humans but not in individuals with type 2 diabetes. *Diabetes*, **49**, 399-408.
28. Firth RG, Bell PM, Marsh HM, Hansen I, Rizza RA 1986 Postprandial hyperglycemia in patients with noninsulin-dependent diabetes mellitus. *J. Clin. Invest*, **77**, 1525-1532.
29. Mari A, Tura A, Pacini G, Kautzky-Willer A, Ferrannini E 2008 Relationships between insulin secretion after intravenous and oral glucose administration in subjects with glucose tolerance ranging from normal to overt diabetes. *Diabet Med.*, **25**, 671.
30. Vaag A, Damsbo P, Hother-Nielsen O, Beck-Nielsen H 1992 Hyperglycaemia compensates for the defects in insulin-mediated glucose metabolism and in the activation of glycogen synthase in the skeletal muscle of patients with type 2 (non-insulin-dependent) diabetes mellitus. *Diabetologia*, **35**, 80-88.
31. Kelley DE, Mandarino LJ 1990 Hyperglycemia normalizes insulin-stimulated skeletal muscle glucose

oxidation and storage in noninsulin-dependent diabetes mellitus. *J. Clin. Invest.*, **86**, 1999-2007.

32. Capaldo B, Santoro D, Riccardi G, Perrotti N, Saccà L 1986 Direct evidence for a stimulatory effect of hyperglycemia per se on peripheral glucose disposal in type II diabetes. *J. Clin. Invest.*, **77**, 1285-1290.
33. Kalant N, Leibovici T, Rohan I, Ozaki S 1979 Interrelationships of glucose and insulin uptake by muscle of normal and diabetic man. Evidence of a difference in metabolism of endogenous and exogenous insulin. *Diabetologia*, **16**, 365-372.
34. Hawkins M, Gabriely I, Wozniak R, Reddy K, Rossetti L, Shamoon H 2002 Glycemic control determines hepatic and peripheral glucose effectiveness in type 2 diabetic subjects. *Diabetes*, **51**, 2179-89.
35. Mevorach M, Giacca A, Aharon Y, Hawkins M, Shamoon H, Rossetti L 1998 Regulation of endogenous glucose production by glucose per se is impaired in type 2 diabetes mellitus. *J. Clin. Invest.*, **102**, 744-753.
36. Nielsen MF, Basu R, Wise S, Caumo A, Cobelli C, Rizza RA 1998 Normal glucose-induced suppression of glucose production but impaired stimulation of glucose disposal in type 2 diabetes: evidence for a concentration dependent defect in uptake. *Diabetes*, **47**, 1735-1747.
37. Del Prato S, Simonson DC, Sheehan P, Cardi F, DeFronzo RA 1997 Studies on the mass effect of glucose in diabetes. Evidence for glucose resistance. *Diabetologia*, **40**, 687-697.
38. Staehr P, Hother-Nielsen O, Levin K, Holst JJ, Beck-Nielsen H 2001 Assessment of hepatic insulin action in obese type 2 diabetic patients. *Diabetes*, **50**, 1363-70.
39. Groop LC, Bonadonna RC, Del Prato S, Ratheiser K, Zyck K, Ferrannini E, DeFronzo RA 1989 Glucose and free fatty acid metabolism in non-insulin-dependent diabetes mellitus. Evidence for multiple sites of insulin resistance. *J. Clin. Invest.*, **84**, 205-213.
40. Campbell PJ, Mandarino LJ, Gerich JE 1988 Quantification of the relative impairment in actions of insulin on hepatic glucose production and peripheral glucose uptake in non-insulin-dependent diabetes mellitus. *Metabolism*, **37**, 15-21.
41. Baron AD, Schaeffer L, Shragg P, Kolterman OG 1987 Role of hyperglucagonemia in maintenance of increased rates of hepatic glucose output in type II diabetics. *Diabetes*, **36**, 274-83.
42. Revers RR, Fink R, Griffin J, Olefsky JM, Kolterman OG (1984) Influence of hyperglycemia on insulin's in vivo effects in type II diabetes. *J. Clin. Invest.*, **73**, 664-672.
43. DeFronzo RA, Simonson D, Ferrannini E 1982 Hepatic and Peripheral Insulin Resistance: A Common Feature of Type 2 (Non-Insulin-Dependent) and Type 1 (Insulin-Dependent) Diabetes Mellitus. *Diabetologia*, **23**, 313-319.
44. Matsuda M, Defronzo RA, Glass L, Consoli A, Giordano M, Bressler P, Delprato S 2002 Glucagon dose-response curve for hepatic glucose production and glucose disposal in type 2 diabetic patients and normal individuals. *Metabolism*, **51**, 1111-1119.
45. Li Y 1993 Centering, trust region, reflective techniques for nonlinear minimization subject to bounds. *Cornell University*.
46. World Health Organization & International Diabetes Federation. 2006 Definition and diagnosis of diabetes mellitus and intermediate hyperglycaemia: report of a WHO/IDF consultation. *World Health Organization*.
47. Sun L, Kwok E, Gopaluni B, Vahidi O. 2011 Pharmacokinetic-Pharmacodynamic Modeling of Metformin for the Treatment of Type II Diabetes Mellitus. *Open Biomed Eng J*, **5**, 1-7.

Figure title and legend

- Figure 1.- Graphical representation of the isolated effects fitted to clinical data of T2DM patients. The solid line represents the isolated effects of (a) M^{I}_{PGU}, (b) M^{G}_{HGP}, (c) $M^{I_\infty}_{HGP}$ and (d) $M^{\Gamma 0}_{HGP}$ after parameter fitting.
- Figure 2.- Graphical representation of the 70g-OGTT. The model considering the $\hat{\theta}$ parameters simulate the blood glucose dynamics after the ingestion of 70 g of glucose at time zero. The solid line represents the model response ((a) x_6 and (b) x_{14}), while the black squares represents the clinical data used to identify the selected parameters of r_{PIR} and taken from DeFronzo *et al.*, [25].
- Figure 3.- Graphical representation of the PGIGI. The T2DM simulate the blood glucose dynamics after the intravenous infusion of glucose at step graded rates. The solid line represents the T2DM model response (x_6), while the black squares represents the clinical data from Carpentier *et al.* [27].

- Figure 4.- Graphical representation of a 25g-OGTT and a 75g-OGTT. The T2DM model simulated the blood glucose dynamics after the ingestion of the respective glucose dose at time zero. The solid and dashed lines represents the model response (x_6) for the 25 g-OGTT and a 75g-OGTT, respectivelly, while the black triangles and squares represents the clinical data from Mari *et al.* [29] and Firth *et al.* [28], respectively.
- Figure 5.- Model Subsystems.- The compartmental diagrams of the (a) glucose, (b) insulin, (c) glucagon and (d) incretins subsystems are shown. The continuous line dividing the subcompartments is used to indicate a low permeability between the walls (*i.e.* variable mass concentration). On the other hand, the dashed line indicate a high permeability, therefore all the sub-compartments in these compartments can be considered as one (*i.e.* uniform mass concentration).
- Figure 6.- General scheme of a compartment. In this representation, there are two well-defined spaces: the capillary blood space and the interstitial fluid space. Among them, there is a low permeability determined by the transcapillary diffusion time T_{AB}. The metabolic rates that add or eliminate the mass of the subsystems are represented by curved arrows entering or leaving the compartments, respectively.

Appendix

Subsystems of the model

A graphical representation of each subsystem of the model in Alverhag and Martin [9] is shown in Figure 5. The glucose an insulin subsystems, *i.e.* in the Figures 5(a) and 5(b), respectively, are divided into several compartments representing organs or tissues interconnected trough blood flow and whose direction is indicated by straight arrows. The subsystems of glucagon and incretins (Figures 5(c) and 5(d), respectively) are divided into one compartment representing the whole body.

A general schematic representation of a compartment is shown in the Figure 6. In this compartment, C_A and C_B represent variables that quantify the concentration of solute in the sub-compartment of capillary blood and the sub-compartment of interstitial fluid, respectively. The quantification of the solute in each compartment is carried out by means of a mass balance. The solute accumulation is a sum of exchange rates (*i.e.* convection and diffusion) while its addition or elimination is due to metabolic rates. The quantification of the solute for the sub-compartment of the figure 6 is given by the following equations:

$$dC_A/dt = (Q_I(C_i - C_A) + \frac{V_B}{T_{AB}}(C_B - C_A))/V_A \tag{10}$$

$$dC_B/dt = (\frac{V_B}{T_{AB}}(C_A - C_B) - r_{sink} + r_{source})/V_B \tag{11}$$

where C_i is the arterial concentration of solute, Q_I, is the volumetric blood flow rate, V_A, and V_B are the blood volume of each sub-compartment and T_B is the transcapillary diffusion time between subcompartments. In what follows, each of these subsystems and its compartments and nomenclature is explained.

Glucose Model

The mass balance in the sub-compartments of the glucose subsystem of the model has given rise to a set of 9 differential equations that are described in Table 5. The glucose subsystem considers 8 metabolic rates: 6 sinks and 2 sources of glucose. The metabolic rates of the brain glucose uptake, red blood cells glucose uptake, and gut glucose uptake are constants. This is $r_{BGU} = \eta_{21}$, $r_{RBCU} = \eta_{22}$ and $r_{GGU} = \eta_{23}$, respectively. The metabolic rates of peripheral glucose uptake (r_{PGU}), hepatic glucose production (r_{HGP}), and hepatic glucose uptake (r_{HGU}) are modeled as multiplicative effects of their basal rate as follows:

1 The multiplicative function r_{PGU} is defined by the equation (4) with $r^B_{PGU} = \eta_{15}$. The function r_{PGU} is mediated just by changes in the insulin and glucose concentrations, then the effect of glucagon in the equation (4) is considered as $M^\Gamma_{PGU} = 1$. The isolated effects of glucose and insulin on the peripheral glucose uptake are determined in Sorensen [10] by fitting the functions to experimental data where M^G_{PGU} is represented as a linear function passing through the origin (*i.e.* $M^G_{PGU} = G_{PI}/G^B_{PI}$) and the function $M^I_{PGU}(I_{PI})$ is determined by the equation (5) with $\eta_j = \{\eta_{17}, \eta_{18}, \eta_{19}, -\eta_{20}\}$.

2 The multiplicative function r_{HGP} is defined by the equation (4) with $r^B_{HGP} = \eta_1$. As the insulin effect on the hepatic glucose production changes from basal to steady state in an exponential way, this function is defined

as:

$$dM^{I}_{HGP}/dt = (M^{I_\infty}_{HGP} - M^{I}_{HGP})/\tau_I \tag{12}$$

The normalized rate of hepatic glucose production resulting from the glucagon step change is modeled by considering the function F_2 that serves to degrade the maximal response of glucagon action to half its initial impact. The above is $M^{\Gamma}_{HGP} = M^{\Gamma_0}_{HGP} - F_2$ where the function F_2 is defined from:

$$dF_2/dt = ((M^{\Gamma_0}_{HGP} - 1)/2 - F_2)/\tau_\Gamma \tag{13}$$

The isolated effect of glucose, the isolated steady state effect of insulin and the initial isolated effect of glucagon on the hepatic glucose production were determined in Sorensen [10] by fitting the functions to clinical data, where $M^{G}_{HGP}(G_L)$, $M^{I_\infty}_{HGP}(I_L)$ and $M^{\Gamma_0}_{HGP}(\Gamma)$ are defined as in the equation (5) with $\eta_j = \{\eta_4, -\eta_5, \eta_6, -\eta_7\}$, $\{0, \eta_2, \eta_3, 0\}$ and $\{\eta_{54}, -\eta_{55}, \eta_{56}, -\eta_{57}\}$, respectively.

3 The multiplicative function r_{HGU} is defined by the equation (4) with $r^{B}_{HGU} = \eta_{11}$. The function r_{HGU} is mediated just by changes in the insulin and glucose concentrations, then the effect of glucagon in the equation (4) is considered as $M^{\Gamma}_{PGU} = 1$. As the time course of mediated hepatic glucose uptake changes from its basal to its steady state value in an exponential manner with time, the function of the isolated effect of insulin is:

$$dM^{I}_{HGU}/dt = (M^{I_\infty}_{HGU} - M^{I}_{HGU})/\tau_I \tag{14}$$

The isolated effect of glucose and the isolated steady state effect of insulin on hepatic glucose uptake are determined in Sorensen [10] by fitting the functions to clinical data, where $M^{G}_{HGU}(G_L)$ and $M^{I_\infty}_{HGU}(I_L)$ are defined by the equation (5) with $\eta_j = \{\eta_8, \eta_{60}, \eta_9, -\eta_{10}\}$ and $\{0, \eta_{52}, \eta_{53}, 0\}$, respectively.

Furthermore, the kidney glucose excretion is modeled as an hyperbolic tangent considering the rate of glucose filtration minus the rate of glucose re-absorption. This is defined as:

$$r_{KGE} = \left\{ \begin{array}{ll} \eta_{12} + \eta_{61} tanh(\eta_{13}(G_K - \eta_{14})) & 0 \le G_K < 460 \\ \eta_{58} + \eta_{59} G_K & G_K \ge 460 \end{array} \right\} \tag{15}$$

The rate of glucose absorption from the intestines into the blood, r_{OGA}, is obtained from the following equation:

$$dr_{OGA}/dt = G_s/(T_A T_{GE}) - r_{OGA}/T_A \tag{16}$$

where the amount of glucose entering the stomach after a meal (OGC_S) depends on the content of carbohydrate of the meal (OGC_O). The above is represented by:

$$\begin{aligned} OGC_s = (OGC_0/\eta_{66})((t-\eta_{66})u(t-\eta_{66}) - (t-\eta_{66}-1)u(t-\eta_{66}-1) \\ - (t-\eta_{66}-4)u(t-\eta_{66}-4) + (t-\eta_{66}-5)u(t-\eta_{66}-5)) \end{aligned} \tag{17}$$

After glucose intake, the gastric emptying process rate describe the rate of glucose transference from the stomach to the intestines by:

$$dG_s/dt = OGCS - G_s/T_{GE} \tag{18}$$

Insulin Subsystem

The graphical representation of the insulin subsystem of the model can be seen in Figure 5(b). The mass balance in the subcompartments has given rise to a set of 8 differential equations that are described in Table 6. In the insulin subsystem, 4 metabolic rates are considered: 3 sinks and 1 source. All the metabolic rates of insulin clearance are

modeled as a fraction of the insulin quantity per minute that an organ receives. This is:
$r_{LIC} = F_{LIC}(Q_A^I I_H + Q_G^I I_G + Q_{PN}^I I_{PN})$, $r_{KIC} = F_{KIC} Q_K^I I_H$ and $r_{PIC} = I_{PI}/(((1 - F_{PIC})/(F_{PIC} Q_P^I)) - T_P^I / V_{PI}^I)$. Whereas, the metabolic rate of pancreatic insulin release (r_{PIR}) is compartmentally modeled to reproduce the two characteristic phases of insulin secretion.
The model to emulate r_{PIR} comes from the fact that one large storage compartment in exchange for insulin with one small compartment. The quantity of insulin in the large compartment is considered constant. Conversely, the quantity of insulin in the small compartment (Q) is considered variable, sensitive to glucose concentration and depending on the rate of insulin exchange between compartments and the insulin secretion rate (S), this is:

$$dQ/dt = \eta_{42}(\eta_{43} - Q) + \eta_{44} P - S \tag{19}$$

where P a function defining the rate of insulin provision from the large compartment to the small one. The above is obtained from:

$$dP/dt = \eta_{35}(P_\infty - P) \tag{20}$$

where P_∞ is the steady state effect of glucose and incretins on insulin release, this is: $P_\infty = Y = X^{\eta_{40}} + \eta_{62}\omega$ and the function X represent an exciter of insulin secretion stimulated by glucose concentration, given by:
$X = G_H/(\eta_{37}^{\eta_{36}} + \eta_{38} G_H^{\eta_{39}})$. Subsequently, the insulin secretion rate is a function defined as:

$$S = (\eta_{46}(X - I)^{0^+} + \eta_{45} Y + \eta_{63}\omega) Q \tag{21}$$

where the notation $(X - I)^{0^+}$ means that the value of the function $X - I$ counts for S when it is positive but it is zero otherwise, and I represent an inhibitory entity (I) of insulin secretion. The last one is obtained from:

$$dI/dt = \eta_{41}(X - I) \tag{22}$$

From the equation (21) can be observed that the first term of the equation represents the first phase of insulin secretion as a proportion of the difference between X and I. Otherwise, the second phase of insulin is obtained from the second term of the equation (21) as the slow transfer of insulin from the large compartment. The above means that it is controlled directly by the provision factor and the amount of labil insulin. Subsequently, the third term of the equation (21) reflects the effect of the concentration of the incretin over insulin release.
The metabolic rate of insulin release is modeled as a scale of the basal insulin secretion rate (r_{PIR}^B) as follows:

$$r_{PIR} = S/S^N r_{PIR}^B \tag{23}$$

where r_{PIR}^B is determined by the fasting insulin concentration in the body as:
$r_{PIR}^B = I_H^B(Q_H^I/(1 - F_{LIC}) - Q_A^I - Q_G^I - (1 - F_{PIC})/(1 - F_{LIC}) Q_P^I - Q_B^I/(1 - F_{LIC}) - Q_K^I(1 - F_{KIC})/(1 - F_{LIC}) - Q_{PN}^I)$.

Glucagon and incretins subsystem

The graphical representation of the glucagon and incretins subsystem can be seen in the figures 5(c) and 5(d), respectively. The mass balance in the sub-compartments has given rise to a set of 3 differential equations described in Table 7. Both subsystems have a metabolic sink, representing the clearance in blood plasma, and a metabolic source, representing release into blood plasma. The rates of glucagon and incretins clearance and the rate of incretins release are modeled as the linear functions: $r_{P\Gamma C} = \eta_{33}\Gamma$, $r_{P\omega C} = r_{M\omega C}\omega$ and $r_{G\omega R} = \omega_G/T_\omega$, respectively. Conversely, the normalized rate of glucagon release ($r_{P\Gamma R}^N$) is modeled as the multiplicative function defined by: $r_{P\Gamma R}^N = M_{P\Gamma R}^G M_{P\Gamma R}^I$. In the above, the isolated effect of glucose ($M_{P\Gamma R}^G(G_H^N)$) and insulin ($M_{P\Gamma R}^I(I_H^N)$) on glucagon release are determined in Sorensen [10] by fitting the equation (5) to experimental data with $\eta_j = \{\eta_{24}, -\eta_{25}, \eta_{26}, -\eta_{27}\}$ and $\eta_j = \{\eta_{28}, -\eta_{29}, \eta_{30}, -\eta_{31}\}$, respectively.

Parameters of the model

The upper and down part of the Table 8 contains all the parameters and its nominal value for the hemodynamical and metabolic processes of the model in Alverhag and Martin [9], respectivelly. For model simulation, when the value of the nominal parameter is considered, then the blood glucose dynamics of a healthy human body is reproduced.

Figures

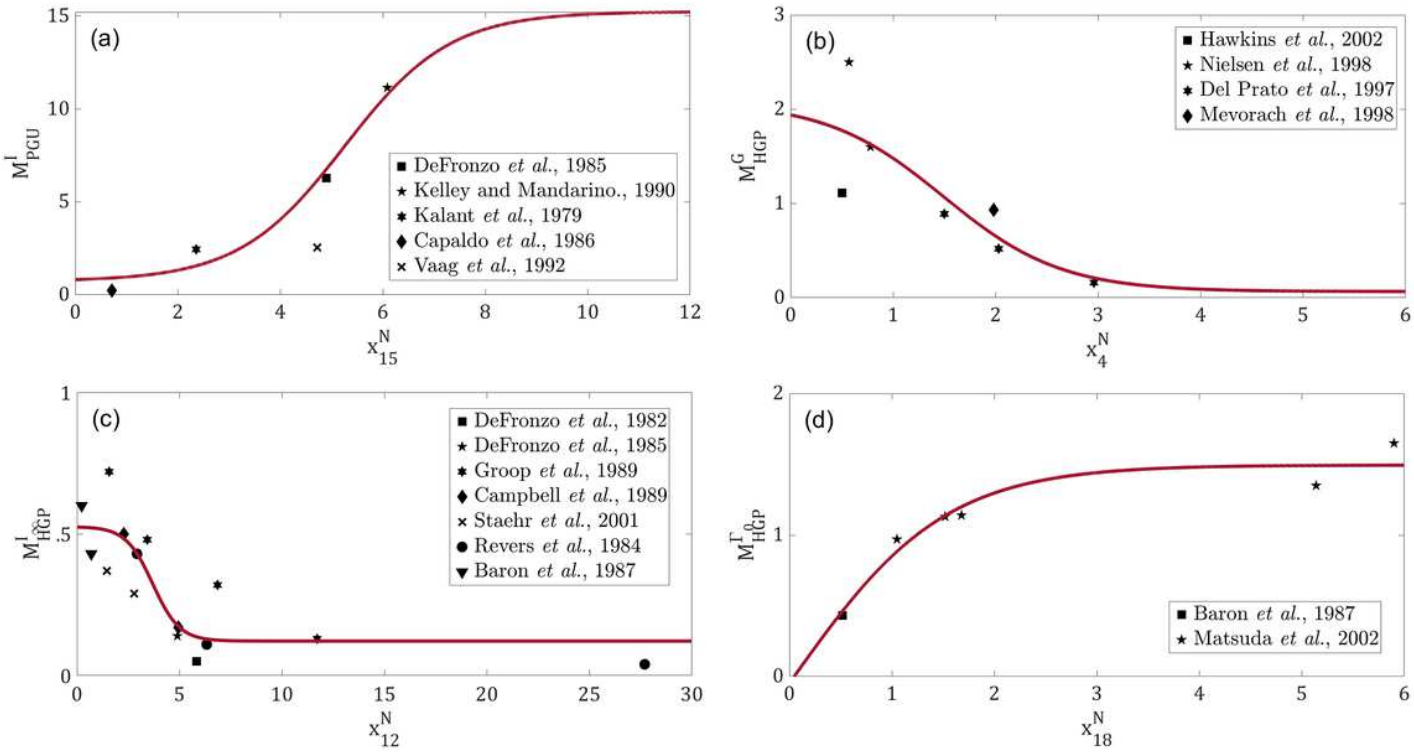

Figure 1

Graphical representation of the isolated effects fitted to clinical data of T2DM patients. The solid line represents the isolated efects of (a) MIPGU , (b) MGHGP, (c) MI¥ HGP and (d) MG0 HGP after parameter fitting.

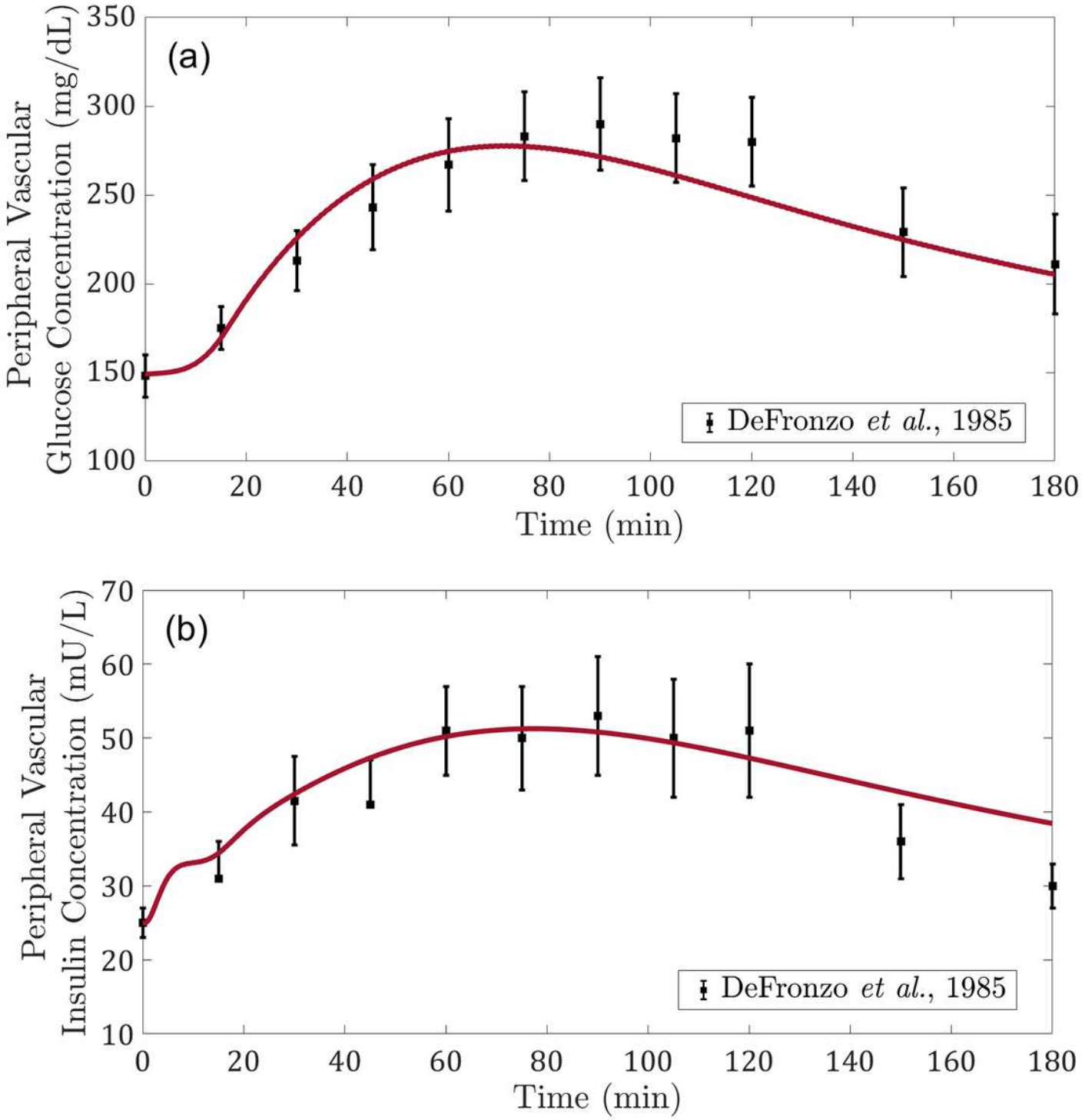

Figure 2

Graphical representation of the 70g-OGTT. The model considering the θˆ parameters simulate the blood glucose dynamics after the ingestion of 70 g of glucose at time zero. The solid line represents the model response ((a) x6 and (b) x14), while the black squares represents the clinical data used to identify the selected parameters of rPIR and taken from DeFronzo et al., [25].

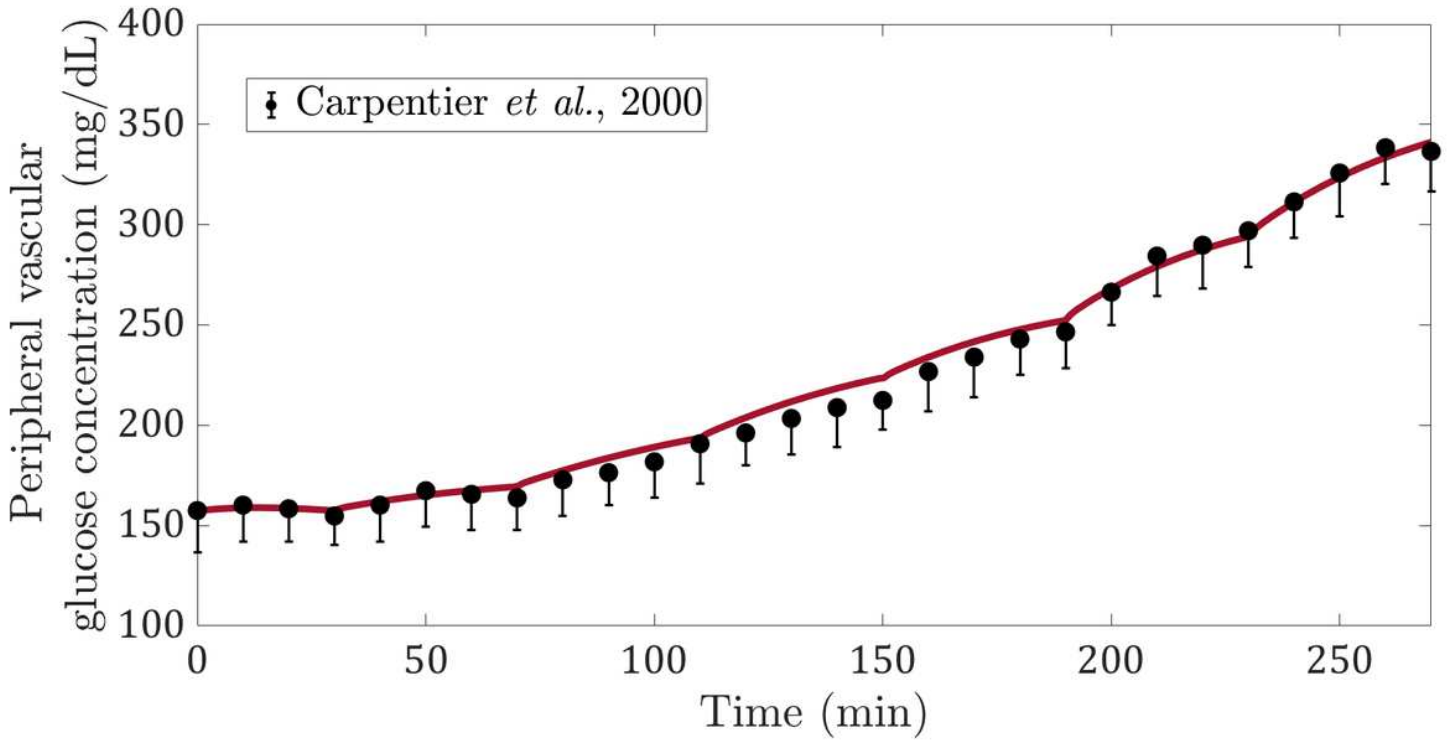

Figure 3

Graphical representation of the PGIGI. The T2DM simulate the blood glucose dynamics after the intravenous infusion of glucose at step graded rates. The solid line represents the T2DM model response (x6), while the black squares represents the clinical data from Carpentier et al. [27].

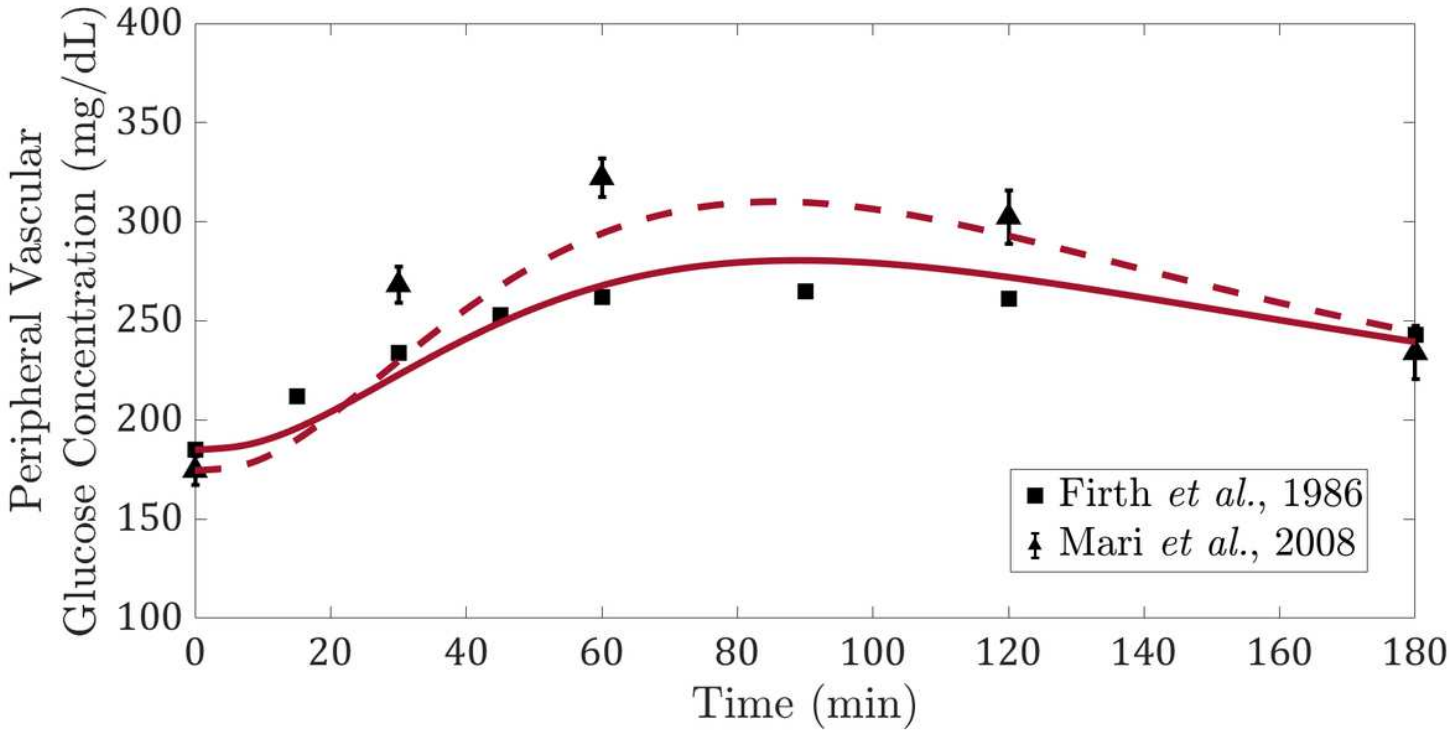

Figure 4

Graphical representation of a 25g-OGTT and a 75g-OGTT. The T2DM model simulated the blood glucose dynamics after the ingestion of the respective glucose dose at time zero. The solid and dashed lines represents the model response (x6) for the 25 g-OGTT and a 75g-OGTT, respectivelly, while the black triangles and squares represents the clinical data from Mari et al. [29] and Firth et al. [28], respectively.

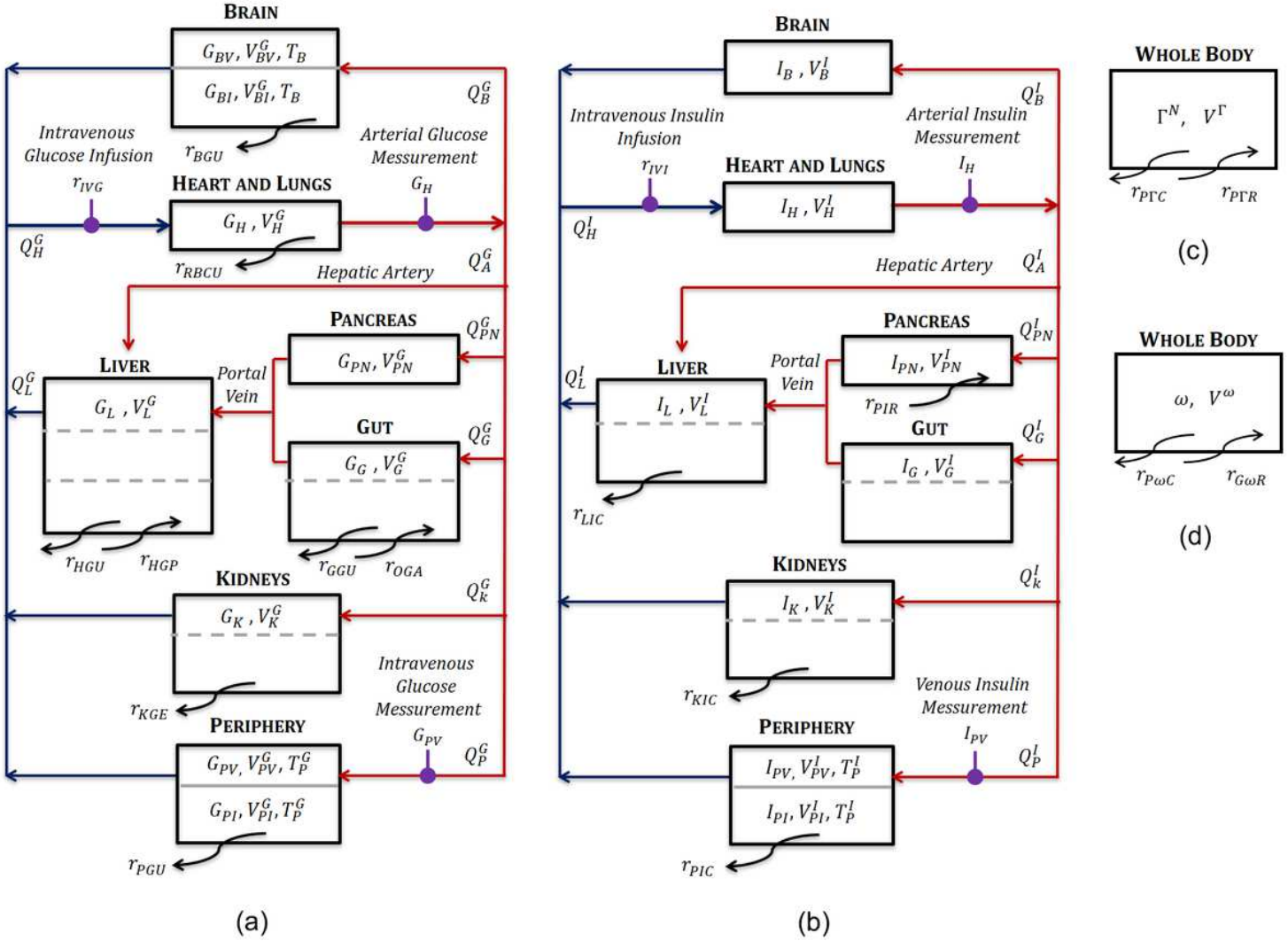

Figure 5

Model Subsystems.- The compartmental diagrams of the (a) glucose, (b) insulin, (c) glucagon and (d) incretins subsystems are shown. The continuous line dividing the subcompartments is used to indicate a low permeability between the walls (i.e. variable mass concentration). On the other hand, the dashed line indicate a high permeability, therefore all the sub-compartments in these compartments can be considered as one (i.e. uniform mass concentration).

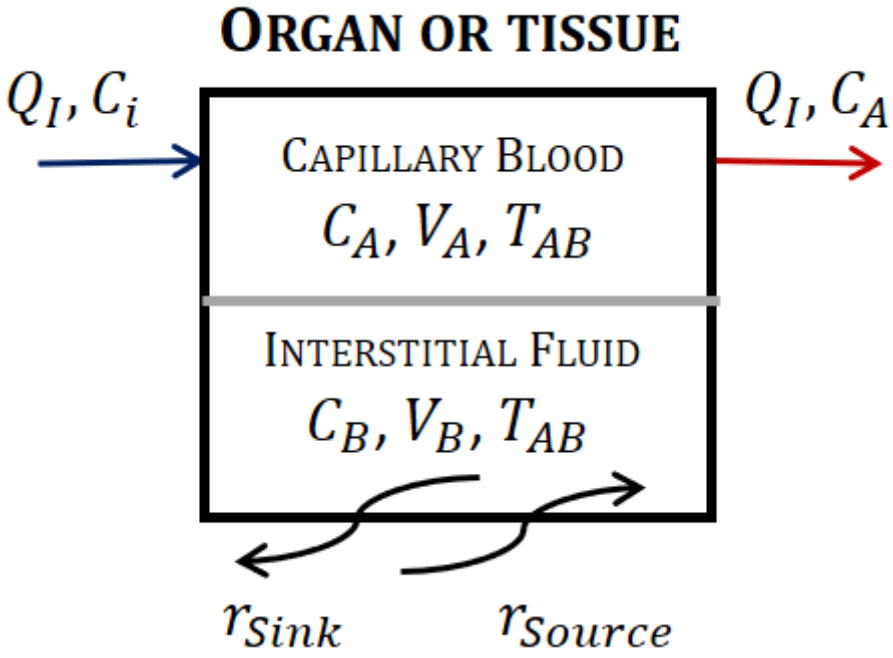

Figure 6

General scheme of a compartment. In this representation, there are two well-dened spaces: the capillary blood space and the interstitial uid space. Among them, there is a low permeability determined by the transcapillary diffusion time TAB. The metabolic rates that add or eliminate the mass of the subsystems are represented by curved arrows entering or leaving the compartments, respectively.

Supplementary Files

This is a list of supplementary files associated with this preprint. Click to download.

- Table7f.xls
- Table3f.xls
- Table4f.xls
- Table6f.xls
- Table1f.xls
- Table2f.xls
- Table5f.xls
- Table8f.xls